



1        **Understanding the Australian Monsoon change during the Last Glacial Maximum**  
2   **with multi-model ensemble**

3                     **Mi Yan<sup>1,2</sup>, Bin Wang<sup>3,4</sup>, Jian Liu<sup>1,2\*</sup>, Axing Zhu<sup>1,2,5,6</sup> and Liang Ning<sup>1,2,7</sup>**

4        1 Key Laboratory of Virtual Geographic Environment, Ministry of Education; State key  
5        Laboratory of Geographical Environment Evolution, Jiangsu Provincial Cultivation Base; School  
6        of Geography Science, Nanjing Normal University, Nanjing, 210023, China.

7        2 Jiangsu Center for Collaborative Innovation in Geographical Information Resource  
8        Development and Application, Nanjing, 210023, China.

9        3 Department of Atmospheric Sciences, University of Hawaii at Manoa, Honolulu, HI 96825,  
10        USA.

11       4 Earth System Modeling Center, Nanjing University of Information Science and Technology,  
12        Nanjing, 210044, China.

13       5 State Key Lab of Resources and Environmental Information System, Institute of Geographic  
14        Sciences and Natural Resources Research, Chinese Academy of Sciences, Beijing, 100101,  
15        China

16       6 Department of Geography, University of Wisconsin-Madison, Madison, WI 53706, USA

17       7 Climate System Research Center, Department of Geosciences, University of Massachusetts,  
18        Amherst, 01003, USA.

19

20       \* Corresponding author address: Dr. Jian Liu, School of Geography Science, Nanjing Normal  
21        University, 1 Wenyuan Road, Nanjing 210023, China

22        E-mail: [jliu@njnu.edu.cn](mailto:jliu@njnu.edu.cn)

23

24



25

### Abstract

26           The response of Australian monsoon to the external forcings and the relative mechanisms  
27 during the Last Glacial Maximum (LGM) is investigated by multi-models in CMIP5/PMIP3.  
28 Although the annual mean precipitation over Australian monsoon region decreases, the annual  
29 range, or the monsoonality, is enhanced. The precipitation increases in early austral summer and  
30 decreases in austral winter, causing the annual range or monsoonality to amplify. The decreased  
31 precipitation in austral winter has a large contribution to the strengthened monsoonality. It is  
32 primarily caused by the weakened upward motion, although the reduced water vapor has also a  
33 moderate contribution. The weakened upward motion in austral winter is induced by the  
34 enhanced land–sea thermal contrast, which intensifies the divergence over northern Australia.  
35 The increased Australian monsoon rainfall in early summer is an integrated result of the positive  
36 effect of local dynamic processes (enhanced moisture convergence) and the negative effect of  
37 thermodynamics (reduced moisture content). The enhanced moisture convergence is caused by  
38 two factors: the strengthened northwest–southeast thermal contrast between the cooler  
39 Indochina–western Indonesia and the warmer northeastern Australia, and the east–west sea  
40 surface temperature gradients between the warmer western Pacific and cooler eastern Indian  
41 Ocean, both due to the alteration of land–sea configuration arising from the sea level drop. The  
42 enhanced Australian monsoonality in LGM is caused by the local processes rather than the large  
43 scale dynamics, which should be taken into account when investigating its future change under  
44 global warming. Our findings may also explain why proxy records indicate different changes in  
45 Australian monsoon precipitation during the LGM.  
46



## 47 **1 Introduction**

48           The changes of the Australian monsoon are crucial for human society and ecology in  
49 Australia (Reeves et al., 2013a), considering the socio-economic importance of monsoon rainfall  
50 (Wang et al., 2017). As the monsoons of the summer hemisphere are linked via outflows from  
51 the opposing winter hemisphere, the Australian monsoon can also influence the Asian–  
52 Indonesian–Australian monsoon system (Eroglu et al., 2016). It is important to understand how  
53 and why the Australian monsoon would change in response to global climate change.

54           With strong climatic forcings (including low greenhouse gas (GHG) concentrations, large  
55 ice-sheets, and low sea level, etc.), the Last Glacial Maximum (LGM) is one of the key periods  
56 that provides an opportunity to better understand the mechanisms of how global and regional  
57 climate response to external forcings (Hewitt et al., 2001; Braconnot et al., 2007; Braconnot et  
58 al., 2011; Harrison et al., 2014). Previous studies have investigated how the external forcing and  
59 boundary conditions during the LGM affected the Intertropical Convergence Zone (ITCZ)  
60 location (Broccoli et al., 2006; Donohoe et al., 2013; McGee et al., 2014), the Walker circulation  
61 (DiNezio et al., 2011), the Indo-Pacific climate (Xu et al., 2010; DiNezio and Tierney, 2013;  
62 DiNezio et al., 2016), the SH circulation (Rojas, 2013), and the global monsoon (Jiang et al.,  
63 2015; Yan et al., 2016). The Australian monsoon onset and variability during the post-glacial, the  
64 late deglaciation, and the Holocene have also been studied using proxy datasets (Ayliffe et al.,  
65 2013; De Deckker et al., 2014; Kuhnt et al., 2015; Bayon et al., 2017). However, due to the  
66 limitation of the scarce proxy datasets, the Australian monsoon change during the LGM is far  
67 from clearly understood.

68           There are different proxy evidences indicating different Australian monsoon change  
69 during the LGM. Here, the Australian monsoon is defined based on the precipitation, i.e., a  
70 strong (weak) monsoon means a wet (dry) condition. Some records show wet conditions over  
71 Australia during the LGM (Ayliffe et al., 2013), while other proxies indicate drier conditions  
72 (Denniston et al., 2013; Denniston et al., 2017; DiNezio and Tierney, 2013). The isotopes from  
73 eggshell of five regions across Australia affirms that Australia becomes drier in the LGM (Miller  
74 et al., 2016), while the speleothem records of southern Australia indicate that it is relatively wet  
75 during the LGM (Treble et al., 2017). The archaeological record showed a refugia-type hunter-  
76 gatherer response over northwest and northeast Australia during the LGM (Williams et al.,



77 2013), indicating that these areas may have had a wetter summer and were therefore preferred by  
78 people as refugia. Bowler et al. (2012) found that the desert dunes advanced while people  
79 upstream feasted on fish and shellfish during the LGM when investigating the lake records over  
80 the southern Australia. The synthesis by the OZ-INTIMATE (Australian INTIMATE,  
81 INTegration of Ice core, MARine and TERrestrial records) project (Turney et al., 2006; Petherick  
82 et al., 2013) showed that the palaeoenvironment over Northern Australia during the LGM was  
83 characterized by drier conditions although wet periods were also noted in the fluvial records  
84 (Reeves et al., 2013a; Reeves et al., 2013b).

85 As one can see from the above description, it is inconclusive on the Australian monsoon  
86 change during the LGM based on proxy data. Therefore, scholars started investigating the  
87 Australian monsoon change from numerical simulation perspectives. The sensitivity of  
88 Australian monsoon to forcings during the late Quaternary has been analyzed using simulations  
89 by Fast Ocean Atmosphere Model (Marshall and Lynch, 2006, 2008). Numerical experiments  
90 have been conducted to analyze the impacts of obliquity and precession with a coupled General  
91 Circulation Model (Wyrwoll et al., 2007) and orbital time-scale circulation with Community  
92 Climate Model (Wyrwoll et al., 2012) on the Australian monsoon. However, different models  
93 may have different responses to the same external forcings, such that the simulated results may  
94 have model dependence. Multi-model ensemble can delineate model biases and therefore provide  
95 more reasonable results of how and why climate system responds to the external forcing  
96 changes.

97 Yan et al (2016) thus used the multi-model ensemble approach to examine the response  
98 of global monsoon to the LGM conditions. It was found that the global monsoon and most sub-  
99 monsoons weakened under the LGM conditions. Some brief hypothesis was made to explain the  
100 changes from global and hemispheric perspectives. The Australian monsoon was thought to be  
101 strengthened due to the southward shift of the ITCZ resulted from the hemispheric thermal  
102 contrast. However, this qualified result of strengthened monsoon or wet condition has not been  
103 proved yet. As mentioned above, it is inconclusive whether the Australian monsoon is  
104 strengthened or not during the LGM. Moreover, Bayon et al. (2017) suggested that the rainfall  
105 pattern in subtropical Australia during the last glacial period was modulated by additional  
106 mechanisms rather than simply the ITCZ. Therefore, model-data and inter-model comparison are



1207 needed and insight studies on the mechanisms are required to better understand the Australian  
1208 monsoon change during the LGM.

1209 This paper will investigate the Australian monsoon change during the LGM and its  
1210 mechanisms from both thermal dynamics and dynamics perspectives, using the multi-model  
1211 ensemble mean derived from models in the fifth phase of the Coupled Model Intercomparison  
1212 Project (CMIP5) (Taylor et al., 2012) and the third phase of the Paleoclimate Modeling  
1213 Intercomparison Project (PMIP3) (Braconnot et al., 2012). We are also trying to quantify the  
1214 contributions of the thermal dynamical and the dynamical processes to the Australian monsoon  
1215 change during the LGM. The models and experiments used in this paper are introduced in Sect.  
1216 2. Section 3 describes simulated results and the physical mechanisms. The comparison with  
1217 proxies and other simulations is discussed in Sect. 4 and the conclusions are made in Sect. 5.

1218

## 1219 **2 Model and Experiments**

1220 Two experiments performed by models participating in CMIP5/PMIP3 are compared in  
1221 this paper: the Last Glacial Maximum Experiment (LGME) and the pre-industrial (PI) control  
1222 run (piControl). The models and experiments are listed in Table 1. To obtain the multi-model  
1223 ensemble (MME), the model outputs were interpolated into a fixed  $2.5^\circ$  (latitude)  $\times$   $2.5^\circ$   
1224 (longitude) grid using the bilinear interpolation method.

1225 The LGM external forcing and boundary conditions are listed in Table 2. More specific  
1226 documentation can be found on the PMIP3 website

1227 (<https://wiki.lsce.ipsl.fr/pmip3/doku.php/pmip3:design:21k:final>).

1228 Compared with the PI, during the LGM the Southern Hemisphere (SH) low latitudes  
1229 ( $30^\circ\text{S-EQ}$ ) receive more insolation from January to August and less from August to December.  
1230 The NH low latitudes ( $\text{EQ-}30^\circ\text{N}$ ) receive less insolation from June to October and more from  
1231 November to May (Fig. S1). Due to the decreased sea level, the landmasses expanded during the  
1232 LGM. A land bridge formed between Indochina and western Indonesia, and the Arafura Sea  
1233 between New Guinea and Australia closed and became landmass (Fig. S2).

1234 The signal-to-noise ratio (S2N) test is used to illustrate the robust changes simulated by  
1235 the different models. The S2N is defined by the ratio of the absolute mean of the MME (as the



136 signal) to the averaged absolute deviation of the individual model against the MME (as the  
137 noise) (Yan et al., 2016). In the following sections, we only consider the areas in which the S2N  
138 ratio exceeds one when we examine the differences between the results derived from the LGME  
139 and piControl.

140

### 141 **3 Results**

142 We defined the difference of precipitation rate between austral summer (DJF) and austral  
143 winter (JJA) as the annual range (AR) to measure the monsoonality of the Australian monsoon.  
144 An increased annual range means a strengthened monsoon. Unlike the South African and South  
145 American monsoon regions (not shown), the monsoonality of the Australian monsoon derived  
146 from the seven models' multi-model ensemble (7MME) is strengthened during the LGM (Fig.  
147 1a). This amplified annual range is the result of increased precipitation in austral summer and  
148 decreased precipitation in austral winter (Fig. 1b). Note that the largest decrease in precipitation  
149 occurred from April to July (late autumn to early winter), not exactly in austral winter; and the  
150 largest increase of precipitation occurred in November and December (ND), i.e., austral early  
151 summer. Since the amount of fall–winter reduction of precipitation exceeds the increased  
152 precipitation in early summer, the annual mean precipitation over the strengthened AR region  
153 decreases by 0.36 mm/day. In summary, while the total annual precipitation decreases in the  
154 LGM, the AR (or the intensity) of the Australian monsoon rainfall is amplified due to seasonal  
155 redistribution of the precipitation, especially the drying in austral fall (April–May) and winter  
156 (JJA) over Australia.

#### 157 3.1 Reasons for the decreased precipitation during the LGM in austral winter (JJA)

158 During the LGM, the lower GHG concentration and the large ice-sheets are the primary  
159 causes for the decreased temperature and the humidity. The global surface specific humidity is  
160 reduced by 2 g/kg (or 20 %) in JJA during the LGM, compared with the PI. For the SH monsoon  
161 regions, the surface specific humidity is more reduced over the Australian monsoon region (by  
162 3.4 g/kg, or 25 %) than the other two monsoon regions (Fig. 2).

163 As suggested by the Clausius–Clapeyron equation, one degree of temperature decrease  
164 would lead to about a 7 % decrease in the saturation water vapor, or roughly the same decrease



165 in the column integrated water vapor. If the circulation remains unchanged, the precipitation  
166 should also be reduced by 7 %. During the LGM, the simulated near surface air temperature over  
167 the Australian monsoon region decreases by 2.5 K in JJA, which implies a decrease of about  
168 17 %. However, the simulated precipitation is reduced by 1.16 mm/day or 58 %, which is far  
169 beyond the value suggested by the thermodynamic effect (approximately 17 %). This suggests  
170 that the majority of the reduction in winter precipitation is due to circulation changes. The  
171 change of the surface wind field shows a strengthened divergence pattern over the Australian  
172 monsoon region (Fig. 3a, vector), which is consistent with the strengthened descending flow over  
173 the Australian monsoon region (Fig. 4) and thus reduced precipitation (Fig. 3a, shading).

174 The JJA mean near surface air temperature shows that the land is cooler than the adjacent  
175 ocean around northern Australia (Fig. 5a), which illustrates a strengthened land–sea thermal  
176 contrast because the land cools more than the ocean surface during the LGM. This strengthened  
177 land–sea contrast leads to a higher sea-level pressure (SLP) over land and lower SLP over ocean  
178 in general (Fig. 5b, shading), and thus the outflows from land (Fig. 5b, vector). The geopotential  
179 height at 850 hPa also shows the relative pattern that matches the wind change (Fig. S3a). The  
180 difference of divergence/convergence field (Fig. 5c) also indicates that the divergence at 850 hPa  
181 over the northern Australia is strengthened during the LGM. The divergence over northern  
182 Australia increased by about 48 %.

183 According to the surface rainfall equation, the precipitation is proportional to the water  
184 vapor content and the low-level convergence (Cui, 2009). Roughly speaking, during the LGM,  
185 the water vapor content is only 80 % of the PI, while the low-level convergence is only 52 % of  
186 the PI, thus the anticipated precipitation should be  $80 \% \times 52 \% = 41.6 \%$ . This means the  
187 anticipated precipitation will decrease by 58.4 %, which is close to the 58 % of the decrease in  
188 the simulated precipitation. In conclusion, both the dynamic process (increased subsidence) and  
189 the thermodynamic process (reduced water vapor content) contribute to the drier winter in the  
190 Australian monsoon region, but the local dynamic processes play a dominant role in the  
191 reduction of Australian winter precipitation.

### 192 3.2 Why the precipitation increased in austral early summer (ND)

193 During ND, the LGM minus PI surface wind difference field shows a strengthened  
194 convergence pattern over the central northern Australian monsoon region (Fig. 6a, vector), which



195 is consistent with the increased precipitation (Fig. 6a, shading). The vertical velocity at 500 hPa  
196 also shows a strengthened ascending flow over this area (Fig. 7). The increased precipitation  
197 over the central Australian monsoon region is clearly against the thermodynamic effects of the  
198 low GHG concentration and the presence of the ice-sheets, which tends to reduce the  
199 precipitation. The 2-m air temperature was decreased by 2.2 K and the surface specific humidity  
200 reduced by 2.6 g/kg (or 16.0 %) over the Australian monsoon region (Fig. 8). The precipitation  
201 would decrease by 15.4 % according to the thermal effect without the circulation change.  
202 However, the precipitation over the Australian monsoon region increased by about 13.0 %.  
203 Therefore, the changes in dynamic processes must induce a 29 % increase of precipitation, so  
204 that the net increase in precipitation reaches 13 %.

205 We noticed that there is a cyclonic wind anomaly associated with an anomalous low  
206 pressure over the northwest Australia (Fig. 6a and Fig. 9b, vector), accompanied by a  
207 strengthened low-level convergence (Fig. 9c), which favors increased precipitation in the  
208 Australian monsoon region. The change of the moisture transport (moisture flux) also indicated  
209 increased moisture transport into northern Australia (not shown). The cyclonic vorticity in  
210 northwest Australia is partially caused by the enhanced strong low-level westerlies that prevail  
211 north of Australia.

212 We now seek to determine why there was a strengthened low-level westerly with  
213 maximum over north of Australia. We first consider the temperature change. The ND mean 2-m  
214 air temperature during the LGM shows that the two enlarged landmasses over the Indo-Pacific  
215 warm pool region (resulting from the lower sea level) change differently (Fig. 9a). It is cooler  
216 over the northwest landmass (western Indonesia–Indochina) and relatively warmer over the  
217 southeast landmass (eastern Indonesia–northern Australia). This temperature variation forms a  
218 southeast–northwest temperature gradient (Fig. 9a), accompanied by a northwest–southeast SLP  
219 gradient (Fig. 9b). The northwest–southeast pressure gradient is stronger in the geopotential  
220 height change at 850 hPa (Fig. S3b). The high pressure in the western Indonesia–Indochina is a  
221 part of the larger scale enhanced winter monsoon over the South China Sea. This enhanced  
222 winter monsoon flows cross the equator from the NH to the SH and turn into strong westerlies  
223 due to deflection induced by the Coriolis force. The 850 hPa convergence strengthens over the  
224 Australian monsoon region (Fig. 9c), and the corresponding ascending motion at 500 hPa also  
225 increases over the Australian monsoon region.





226 Another reason for circulation change is the sea surface temperature (SST) gradient  
227 change. The SST anomaly in ND shows a warmer Western Pacific and cooler Eastern Indian  
228 Ocean pattern (Fig. 10), indicating a westward temperature gradient, and thus an eastward  
229 pressure gradient which, in the equatorial region, can directly enhance westerly winds near the  
230 northern Australian monsoon region (Fig. 9b). Li et al. (2012) also found that a cold state of the  
231 Wharton Basin (100–130°E, 20–5°S) was accompanied by anomalous westerlies and cyclonic  
232 circulation anomalies in the Australian monsoon region, which were associated with a strong  
233 tropical Australian summer monsoon and enhanced rainfall over northeast Australia.

234 In summary, during ND, the enlarged land area due to sea-level drop enhances the land–  
235 sea thermal contrast, and forms a northwest–southeast thermal contrast which induces low  
236 pressure over northern Australia but high pressure over the adjacent ocean and the Indochina–  
237 western Indonesia, leading to enhanced convergence over northern Australia and thus increasing  
238 the early summer monsoon rainfall. The SST gradients between the warm equatorial western  
239 Pacific and relatively cool eastern Indian Ocean during the pre-summer monsoon season also  
240 contribute to the strengthened equatorial westerlies and the cyclonic wind anomaly over northern  
241 Australia. These dynamic mechanisms have a positive contribution to the early summer  
242 precipitation (nearly 29 %). The thermal effects have negative contribution to the precipitation  
243 change by about 16 %. Therefore, the early summer precipitation over northern Australia  
244 increases by about 13 %.

245

#### 246 **4 Discussion**

247 The intensification of the Australian monsoon in this study is measured by the enhanced  
248 seasonal difference (or the seasonality) of precipitation, and is particularly attributed to the  
249 decreased austral winter precipitation. Whereas the annual mean precipitation is decreased,  
250 which means the Australian monsoon would be weakened during the LGM when it is measured  
251 by the annual mean precipitation. The modeling study by DiNezio et al. (2013) suggests a  
252 decreasing rainfall across northern Australia during the LGM, consistent with the proxy  
253 synthesis by stalagmite (Denniston et al., 2017). The decreased rainfall in their work represents  
254 the annual mean precipitation, which also consists with our work in this point of view. On the  
255 other hand, the increased rainfall in austral summer in this study is consistent with what has been



256 revealed in the reconstructed work by Liu et al. (2015) (Shen CC, personal communication,  
257 2017).

258           The decreased annual mean precipitation and the intensified seasonality of precipitation  
259 over the Australian monsoon region is in agreement with the synthesis from the simulated result  
260 by Tharammal et al. (2013) using a set of experiments. In their work, the seasonality is  
261 calculated by the difference between boreal summer (JJA) and boreal winter (DJF), and the  
262 difference of the seasonality over the Australian monsoon region between the LGM and the PI is  
263 negative. Regarding to their negative value during the PI, the seasonality of precipitation over the  
264 Australian monsoon region is actually enhanced during the LGM, which also indicates an  
265 intensified Australian monsoon.

266           For the forcings and mechanisms of the Australian monsoon change during the LGM,  
267 there are large changes in four external forcings during the LGM, including the insolation change  
268 resulting from the orbital change, the land–sea configuration change, the GHG change and the  
269 presence of ice-sheets. The lower GHG concentrations and the presence of ice-sheets are likely  
270 to be contributors to the thermal effect leading to the reduced water vapor and thus the decreased  
271 rainfall both in austral winter and early summer. The enlarged the landmasses over western  
272 Indonesia and northeastern Australia are essential to the local dynamic processes that influence  
273 the rainfall. The low obliquity and high precession during the LGM may be another factor that  
274 can affect the rainfall (Liu et al., 2015). However, the impact of the insolation change caused by  
275 the orbital change remains unknown.

276           During the LGM, the insolation over tropical region increased from December to June  
277 and decreased from July to November (Fig. 11a). The precipitation change would lag the  
278 insolation change by about two months, due to the ocean–atmosphere interaction without other  
279 processes. For example, the change of seasonal distribution of NH monsoon precipitation lagged  
280 the change of the NH insolation by one month (Yan et al., 2016). Whereas in this study, the  
281 Australian monsoon precipitation decreased from March to September and increased from  
282 November to February (Fig. 11b), quite different from what it would be (i.e., decrease from  
283 September to January and increase from February to August). Meanwhile, the insolation over SH  
284 increased during the LGM from April to August, when Australia is in late fall and winter. An  
285 increased insolation might make land warmer than ocean thus against the climatology, which



286 may be described by cooler land and warmer ocean in winter. However, the simulated surface  
287 temperature reduced more over Australia than the adjacent oceans (Fig. 5a). On the other hand,  
288 the synthesis of Wyrwoll et al. (2007) and Liu et al. (2015) indicates the strong convergence rain  
289 belt stays in the north, resulting in more rainfall over Papua New Guinea and less rainfall over  
290 North Australia during those times with low obliquity and high precession. The rain belt stays a  
291 little more northerly than that stays in our study, which means the effect of orbital change and  
292 thus the insolation change might be suppressed by other factors.

293 Moreover, the paleoclimate records suggest that it was dry and cool in the Indo-Pacific  
294 Warm Pool region during the LGM (Xu et al., 2010). The simulated SST is consistent with the  
295 reconstructions. Although in the early austral summer, over the Indian Ocean warm pool, it is  
296 cooler over the SH, while over the Pacific warm pool, it is cooler over the NH (Fig. S4). Such  
297 anomalous SST asymmetry may favor the southward shift of the ITCZ over Australia and the  
298 southwest Pacific, which might be related to the enhanced austral summer monsoon  
299 precipitation. However, the 7MME shows no significant ITCZ shift during the LGM, particularly  
300 over the central Australian monsoon region (Fig. S5). McGee et al. (2014) also found that the  
301 ITCZ shifted no more than 1° latitude during the LGM.

302 Therefore, it is the local dynamical processes, instead of the large-scale circulation such  
303 as the position of the ITCZ induced by the NH-SH thermal contrast, that might be the key factor  
304 influencing the early summer mean precipitation change over the Australian monsoon region  
305 during the LGM.

## 306 **5 Conclusions**

307 The temperature and water vapor have an overall decrease under the LGM forcings  
308 (lower GHG and large ice-sheets). Nevertheless, the simulated Australian monsoon derived from  
309 CMIP5/PMIP3 multi-model ensemble has a distinctive amplification (or the monsoonality is  
310 intensified) against the weakened global monsoons elsewhere during the LGM. This study then  
311 investigated the possible reasons for this strengthened Australian monsoonality in thermal  
312 dynamical and dynamical perspective.

313 The conclusions are as follows and the relative mechanisms are shown in Fig. 12:



- 314 1) The Australian monsoon is strengthened as a result of the enhanced seasonal difference  
315 between austral summer and winter, i.e., the increased early summer (ND) mean  
316 rainfall and the reduced winter (JJA) mean rainfall. Both the dynamic processes and  
317 thermal effects contribute to the precipitation change; however, the dynamic processes  
318 have a much stronger contribution than the thermal effects.
- 319 2) The Australian winter monsoon (JJA mean) precipitation decreased by 58 % during the  
320 LGM relative to the preindustrial control experiment. The dynamic processes, induced  
321 by the enhanced land–ocean thermal contrast, contribute to a decrease of about 48 %  
322 through the strengthened divergence over northern Australia, whereas the thermal effect  
323 (i.e., the reduced atmospheric water vapor due to the lower temperature induced by  
324 lower GHGs and present ice-sheets) has a moderate contribution of nearly 20 %.
- 325 3) For the increased precipitation in early summer (ND), the local dynamic processes  
326 contribute +29 % and the thermal effect contributes –16 %. Correspondingly, the ND  
327 precipitation increases by about 13 %. The local dynamic processes are mainly induced  
328 by the northwest–southeast thermal contrast between Indochina–western Indonesia and  
329 northeastern Australia. The east Indian Ocean–west Pacific Ocean thermal gradient also  
330 contributes to these processes.
- 331 4) The change in circulation over Australia and South Asia are very likely to be rooted in  
332 the enlarged landmasses over the Indochina–western Indonesia and New Guinea, and  
333 northern Australia. Changes of the land–ocean configuration has a critical impact on the  
334 thermal gradients that induce changes in the low-level circulation pattern and  
335 convergence/divergence.

336 Our results are based on the equilibrium simulation, representing a synthesized mean  
337 state of the Australian monsoon change and its possible mechanisms during the LGM. More  
338 simulations with single forcing (such as the SST asymmetry change, the insolation change, and  
339 the landmass change) are required to further understand the effect of each factor and to  
340 specifically quantify the contribution of each forcing to the Australian monsoon change.  
341



342 **Acknowledgments**

343 We acknowledge Prof. Williams J for the comments helping to clarify and improve the  
344 paper. This research was jointly supported by the National Key Research and Development  
345 Program of China (Grant No. 2016YFA0600401), the National Basic Research Program (Grant  
346 No. 2015CB953804), the National Natural Science Foundation of China (Grant Nos. 41671197,  
347 41420104002 and 41501210), and the Priority Academic Development Program of Jiangsu  
348 Higher Education Institutions (PAPD, Grant No. 164320H116). We acknowledge the World  
349 Climate Research Programme's Working Group on Coupled Modeling, which is responsible for  
350 the CMIP, and we thank the climate modeling groups for producing and making available their  
351 model outputs. For the CMIP, the U.S. Department of Energy's Program for climate model  
352 diagnosis and intercomparison provided coordinating support and led the development of  
353 software infrastructure in partnership with the Global Organization for Earth System Science  
354 Portals. We thank LetPub ([www.letpub.com](http://www.letpub.com)) for its linguistic assistance during the preparation  
355 of this manuscript.

356



357 **References**

- 358 Ayliffe, L. K., Gagan, M. K., Zhao, J. X., Drysdale, R. N., Hellstrom, J. C., Hantoro, W. S.,  
359 Griffiths, M. L., Scott-Gagan, H., St Pierre, E., Cowley, J. A., and Suwargadi, B. W.: Rapid  
360 interhemispheric climate links via the Australasian monsoon during the last deglaciation,  
361 Nat Commun, 4, 2908, 10.1038/ncomms3908, 2013.
- 362 Bayon, G., De Deckker, P., Magee, J. W., Germain, Y., Bermell, S., Tachikawa, K., and  
363 Norman, M. D.: Extensive wet episodes in Late Glacial Australia resulting from high-  
364 latitude forcings, Scientific Reports, 7, 44054, 10.1038/srep44054, 2017.
- 365 Bowler, J. M., Gillespie, R., Johnston, H., and Boljkovac, K.: Wind v water: Glacial maximum  
366 records from the Willandra Lakes, in: Peopled Landscapes: Archaeological and  
367 Biogeographic Approaches to Landscapes, edited by: Haberle, S., and David, B., ANU E  
368 Press, Canberra, Australia, 271-296, 2012.
- 369 Braconnot, P., Otto-Bliesner, B., Harrison, S. P., and al, e.: Results of PMIP2 coupled  
370 simulations of the Mid-Holocene and Last Glacial Maximum – Part 2: feedbacks with  
371 emphasis on the location of the ITCZ and mid- and high latitudes heat budget, Climate of  
372 the Past, 3, 2007.
- 373 Braconnot, P., Harrison, S. P., Kageyama, M., Bartlein, P. J., Masson-Delmotte, V., Abe-Ouchi,  
374 A., Otto-Bliesner, B., and Zhao, Y.: Evaluation of climate models using palaeoclimatic data,  
375 Nature Climate Change, 2, 417-424, 10.1038/nclimate1456, 2012a.
- 376 Braconnot, P., Harrison, S. P., Otto-Bliesner, B., Abe-Ouchi, A., Jungclaus, J., and Peterschmitt,  
377 J. Y.: The Paleoclimate Modeling Intercomparison Project contribution to CMIP5, CLIVAR  
378 Exchanges, 56, 15-19, 2012b.
- 379 Broccoli, A. J., Dahl, K. A., and Stouffer, R. J.: Response of the ITCZ to Northern Hemisphere  
380 cooling, Geophysical Research Letters, 33(1), L01702, 10.1029/2005gl024546, 2006.
- 381 Cui, X. P.: Quantitative diagnostic analysis of surface rainfall processes by surface rainfall  
382 equation. Chinese Journal of Atmospheric Sciences, 33(2), 375–387, 2009.
- 383 De Deckker, P., Barrows, T. T., and Rogers, J.: Land–sea correlations in the Australian region:  
384 post-glacial onset of the monsoon in northwestern Western Australia, Quaternary Science  
385 Reviews, 105, 181-194, 10.1016/j.quascirev.2014.09.030, 2014.



- 386 Denniston, R. F., Wyrwoll, K.-H., Asmerom, Y., Polyak, V. J., Humphreys, W. F., Cugley, J.,  
387 Woods, D., LaPointe, Z., Peota, J., and Greaves, E.: North Atlantic forcing of millennial-  
388 scale Indo-Australian monsoon dynamics during the Last Glacial period, *Quaternary*  
389 *Science Reviews*, 72, 159-168, [10.1016/j.quascirev.2013.04.012](https://doi.org/10.1016/j.quascirev.2013.04.012), 2013.
- 390 Denniston, R. F., Asmerom, Y., Polyak, V. J., Wanamaker, A. D., Ummenhofer, C. C.,  
391 Humphreys, W. F., Cugley, J., Woods, D., and Lucker, S.: Decoupling of monsoon activity  
392 across the northern and southern Indo-Pacific during the Late Glacial, *Quaternary Science*  
393 *Reviews*, 176, 101-105, [10.1016/j.quascirev.2017.09.014](https://doi.org/10.1016/j.quascirev.2017.09.014), 2017.
- 394 DiNezio, P. N., Timmermann, A., Tierney, J. E., Jin, F.-F., Otto-Bliesner, B., Rosenbloom, N.,  
395 Mapes, B., Neale, R., Ivanovic, R. F., and Montenegro, A.: The climate response of the  
396 Indo-Pacific warm pool to glacial sea level, *Paleoceanography*, 31, 866-894,  
397 [10.1002/2015PA002890](https://doi.org/10.1002/2015PA002890), 2016.
- 398 DiNezio, P. N., Clement, A., Vecchi, G. A., Soden, B., Broccoli, A. J., Otto-Bliesner, B. L., and  
399 Braconnot, P.: The response of the Walker circulation to Last Glacial Maximum forcing:  
400 Implications for detection in proxies, *Paleoceanography*, 26, n/a-n/a,  
401 [10.1029/2010pa002083](https://doi.org/10.1029/2010pa002083), 2011.
- 402 DiNezio, P. N., and Tierney, J. E.: The effect of sea level on glacial Indo-Pacific climate, *Nature*  
403 *Geoscience*, 6, 485-491, [10.1038/ngeo1823](https://doi.org/10.1038/ngeo1823), 2013.
- 404 Donohoe, A., Marshall, J., Ferreira, D., and McGee, D.: The Relationship between ITCZ  
405 Location and Cross-Equatorial Atmospheric Heat Transport: From the Seasonal Cycle to  
406 the Last Glacial Maximum, *Journal of Climate*, 26, 3597-3618, [10.1175/jcli-d-12-00467.1](https://doi.org/10.1175/jcli-d-12-00467.1),  
407 2013.
- 408 Eroglu, D., McRobie, F. H., Ozken, I., Stemler, T., Wyrwoll, K. H., Breitenbach, S. F., Marwan,  
409 N., and Kurths, J.: See-saw relationship of the Holocene East Asian-Australian summer  
410 monsoon, *Nat Commun*, 7, 12929, [10.1038/ncomms12929](https://doi.org/10.1038/ncomms12929), 2016.
- 411 Hargreaves, J. C., Annan, J. D., Ohgaito, R., Paul, A., and Abe-Ouchi, A.: Skill and reliability of  
412 climate model ensembles at the Last Glacial Maximum and mid-Holocene, *Climate of the*  
413 *Past*, 9, 811-823, [10.5194/cp-9-811-2013](https://doi.org/10.5194/cp-9-811-2013), 2013.



- 414 Harrison, S. P., Bartlein, P. J., Brewer, S., Prentice, I. C., Boyd, M., Hessler, I., Holmgren, K.,  
415 Izumi, K., and Willis, K.: Climate model benchmarking with glacial and mid-Holocene  
416 climates, *Climate Dynamics*, 43, 671-688, [10.1007/s00382-013-1922-6](https://doi.org/10.1007/s00382-013-1922-6), 2014.
- 417 Hewitt, C., Broccoli, A. J., Mitchell, J. F. B., and Stouffer, R.: A coupled model study of the last  
418 glacial maximum: Was part of the North Atlantic relatively warm? *Geophys. Res. Lett.*, 28,  
419 1571-1574, 2001.
- 420 Jiang, D., Tian, Z., Lang, X., Kageyama, M., and Ramstein, G.: The concept of global monsoon  
421 applied to the last glacial maximum: A multi-model analysis, *Quaternary Science Reviews*,  
422 126, 126-139, [10.1016/j.quascirev.2015.08.033](https://doi.org/10.1016/j.quascirev.2015.08.033), 2015.
- 423 Kuhnt, W., Holbourn, A., Xu, J., Opdyke, B., De Deckker, P., Rohl, U., and Mudelsee, M.:  
424 Southern Hemisphere control on Australian monsoon variability during the late deglaciation  
425 and Holocene, *Nat Commun*, 6, 5916, [10.1038/ncomms6916](https://doi.org/10.1038/ncomms6916), 2015.
- 426 Li, J., Feng, J., and Li, Y.: A possible cause of decreasing summer rainfall in northeast Australia,  
427 *International Journal of Climatology*, 32, 995-1005, [10.1002/joc.2328](https://doi.org/10.1002/joc.2328), 2012.
- 428 Liu, Y., Lo, L., Shi, Z., Wei, K. Y., Chou, C. J., Chen, Y. C., Chuang, C. K., Wu, C. C., Mii, H.  
429 S., Peng, Z., Amakawa, H., Burr, G. S., Lee, S. Y., DeLong, K. L., Elderfield, H., and Shen,  
430 C. C.: Obliquity pacing of the western Pacific Intertropical Convergence Zone over the past  
431 282,000 years, *Nat Commun*, 6, 10018, [10.1038/ncomms10018](https://doi.org/10.1038/ncomms10018), 2015.
- 432 Marshall, A. G., and Lynch, A. H.: Time-slice analysis of the Australian summer monsoon  
433 during the late Quaternary using the Fast Ocean Atmosphere Model, *Journal of Quaternary  
434 Science*, 21, 789-801, [10.1002/jqs.1063](https://doi.org/10.1002/jqs.1063), 2006.
- 435 Marshall, A. G., and Lynch, A. H.: The sensitivity of the Australian summer monsoon to climate  
436 forcing during the late Quaternary, *Journal of Geophysical Research*, 113,  
437 [10.1029/2007jd008981](https://doi.org/10.1029/2007jd008981), 2008.
- 438 McGee, D., Donohoe, A., Marshall, J., and Ferreira, D.: Changes in ITCZ location and cross-  
439 equatorial heat transport at the Last Glacial Maximum, Heinrich Stadial 1, and the mid-  
440 Holocene, *Earth and Planetary Science Letters*, 390, 69-79, [10.1016/j.epsl.2013.12.043](https://doi.org/10.1016/j.epsl.2013.12.043),  
441 2014.





- 442 Miller, G. H., Fogel, M. L., Magee, J. W., and Gagan, M. K.: Disentangling the impacts of  
443 climate and human colonization on the flora and fauna of the Australian arid zone over the  
444 past 100 ka using stable isotopes in avian eggshell, *Quaternary Science Reviews*, 151, 27-  
445 57, 10.1016/j.quascirev.2016.08.009, 2016.
- 446 Petherick, L., Bostock, H., Cohen, T. J., Fitzsimmons, K., Tibby, J., Fletcher, M. S., Moss, P.,  
447 Reeves, J., Mooney, S., Barrows, T., Kemp, J., Jansen, J., Nanson, G., and Dosseto, A.:  
448 Climatic records over the past 30 ka from temperate Australia – a synthesis from the Oz-  
449 INTIMATE workgroup, *Quaternary Science Reviews*, 74, 58-77,  
450 10.1016/j.quascirev.2012.12.012, 2013.
- 451 Reeves, J. M., Barrows, T. T., Cohen, T. J., Kiem, A. S., Bostock, H. C., Fitzsimmons, K. E.,  
452 Jansen, J. D., Kemp, J., Krause, C., Petherick, L., and Phipps, S. J.: Climate variability over  
453 the last 35,000 years recorded in marine and terrestrial archives in the Australian region: an  
454 OZ-INTIMATE compilation, *Quaternary Science Reviews*, 74, 21-34,  
455 10.1016/j.quascirev.2013.01.001, 2013a.
- 456 Reeves, J. M., Bostock, H. C., Ayliffe, L. K., Barrows, T. T., De Deckker, P., Devriendt, L. S.,  
457 Dunbar, G. B., Drysdale, R. N., Fitzsimmons, K. E., Gagan, M. K., Griffiths, M. L.,  
458 Haberle, S. G., Jansen, J. D., Krause, C., Lewis, S., McGregor, H. V., Mooney, S. D., Moss,  
459 P., Nanson, G. C., Purcell, A., and van der Kaars, S.: Palaeoenvironmental change in  
460 tropical Australasia over the last 30,000 years – a synthesis by the OZ-INTIMATE group,  
461 *Quaternary Science Reviews*, 74, 97-114, 10.1016/j.quascirev.2012.11.027, 2013b.
- 462 Rojas, M.: Sensitivity of Southern Hemisphere circulation to LGM and  $4 \times \text{CO}_2$  climates,  
463 *Geophysical Research Letters*, 40, 965-970, 10.1002/grl.50195, 2013.
- 464 Taylor, K. E., Stouffer, R. J., and Meehl, G. A.: An Overview of CMIP5 and the Experiment  
465 Design, *Bulletin of the American Meteorological Society*, 93, 485-498, 10.1175/bams-d-11-  
466 00094.1, 2012.
- 467 Tharammal, T., Paul, A., Merkel, U., and Noone, D.: Influence of Last Glacial Maximum  
468 boundary conditions on the global water isotope distribution in an atmospheric general  
469 circulation model, *Climate of the Past*, 9, 789-809, 10.5194/cp-9-789-2013, 2013. Treble, P.  
470 C., Baker, A., Ayliffe, L. K., Cohen, T. J., Hellstrom, J. C., Gagan, M. K., Frisia, S.,



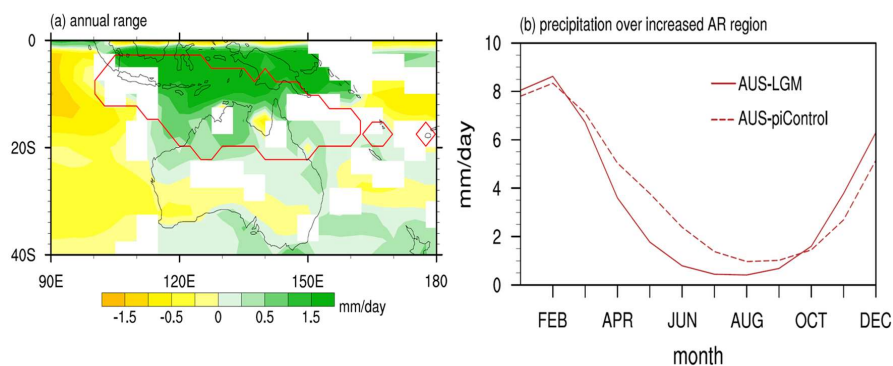
- 471 Drysdale, R. N., and Griffiths, A. D.: Hydroclimate of the Last Glacial Maximum and  
472 deglaciation in southern Australia's arid margin interpreted from speleothem records (23-15  
473 ka), *Climate of the Past*, 13, 667-687, 2017.
- 474 Treble, P. C., Baker, A., Ayliffe, L. K., Cohen, T. J., Hellstrom, J. C., Gagan, M. K., Frisia, S.,  
475 Drysdale, R. N., and Griffiths, A. D.: Hydroclimate of the Last Glacial Maximum and  
476 deglaciation in southern Australia's arid margin interpreted from speleothem records (23-15  
477 ka), *Climate of the Past*, 13, 667-687, 2017.
- 478 Turney, C. S. M., Haberle, S., Fink, D., Kershaw, A. P., Barbetti, M., Barrows, T. T., Black, M.,  
479 Cohen, T. J., Corrège, T., Hesse, P. P., Hua, Q., Johnston, R., Morgan, V., Moss, P.,  
480 Nanson, G., van Ommen, T., Rule, S., Williams, N. J., Zhao, J. X., D'Costa, D., Feng, Y.  
481 X., Gagan, M., Mooney, S., and Xia, Q.: Integration of ice-core, marine and terrestrial  
482 records for the Australian Last Glacial Maximum and Termination: a contribution from the  
483 OZ INTIMATE group, *Journal of Quaternary Science*, 21, 751-761, 10.1002/jqs.1073,  
484 2006.
- 485 Wang, P. X., Wang, B., Cheng, H., Fasullo, J., Guo, Z., Kiefer, T., and Liu, Z.: The global  
486 monsoon across time scales: Mechanisms and outstanding issues, *Earth-Science Reviews*,  
487 10.1016/j.earscirev.2017.07.006, 2017.
- 488 Williams, A. N., Ulm, S., Cook, A. R., Langley, M. C., and Collard, M.: Human refugia in  
489 Australia during the Last Glacial Maximum and Terminal Pleistocene: a geospatial analysis  
490 of the 25–12 ka Australian archaeological record, *Journal of Archaeological Science*, 40,  
491 4612-4625, 10.1016/j.jas.2013.06.015, 2013.
- 492 Wyrwoll, K.-H., Liu, Z., Chen, G., Kutzbach, J. E., and Liu, X.: Sensitivity of the Australian  
493 summer monsoon to tilt and precession forcing, *Quaternary Science Reviews*, 26, 3043-  
494 3057, 10.1016/j.quascirev.2007.06.026, 2007.
- 495 Wyrwoll, K.-H., Hopwood, J. M., and Chen, G.: Orbital time-scale circulation controls of the  
496 Australian summer monsoon: a possible role for mid-latitude Southern Hemisphere forcing?  
497 *Quaternary Science Reviews*, 35, 23-28, 10.1016/j.quascirev.2012.01.003, 2012.



- 498 Xu, J., Kuhnt, W., Holbourn, A., Regenberg, M., and Andersen, N.: Indo-Pacific Warm Pool  
499 variability during the Holocene and Last Glacial Maximum, *Paleoceanography*, 25,  
500 10.1029/2010pa001934, 2010.
- 501 Yan, M., Wang, B., and Liu, J.: Global monsoon change during the Last Glacial Maximum: a  
502 multi-model study, *Climate Dynamics*, 47, 359-374, 10.1007/s00382-015-2841-5, 2016.  
503



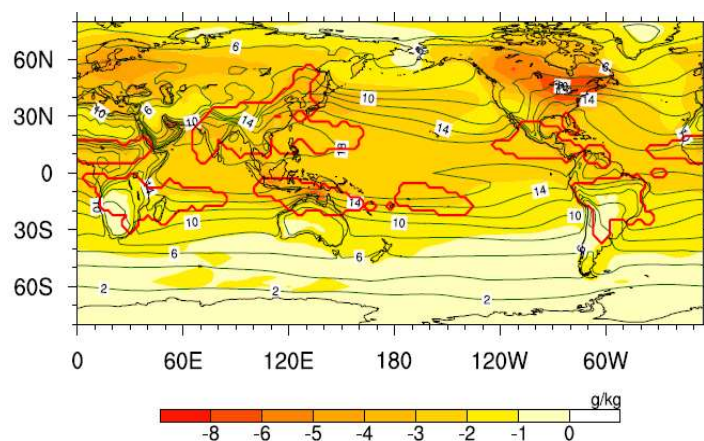
504



505

506 **Figure 1** (a) Spatial distribution of changes in the annual range of precipitation measured by the  
 507 difference between LGME and piControl, and (b) annual cycle of the precipitation in the  
 508 increased annual range region over the Australian monsoon. The red solid line in (a) encloses the  
 509 Australian monsoon rainfall domain. The dashed (solid) line in (b) denotes the seasonal  
 510 distribution of precipitation derived from the piControl (LGME) run. Only those areas where  
 511 signal-to-noise ratio exceeds one are plotted in (a).

512

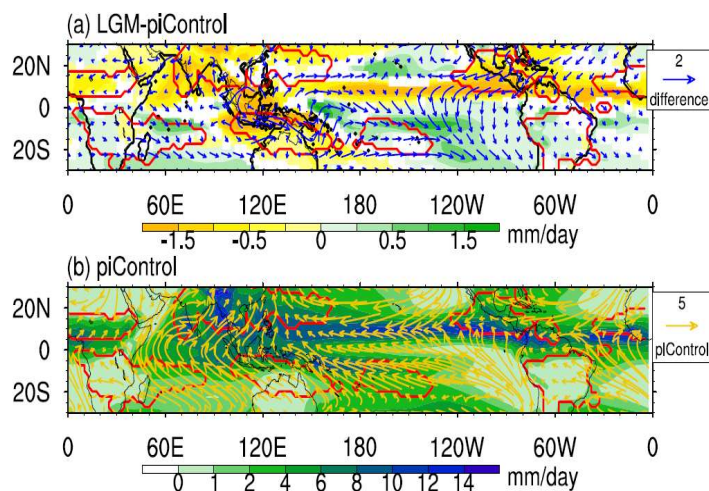


513

514 **Figure 2** Difference of JJA mean surface specific humidity between LGME and piControl  
 515 (shaded). The green contours denote the climatology derived from piControl. The red lines  
 516 enclose the monsoon domains. Only those areas where signal-to-noise ratio exceeds one are  
 517 plotted.



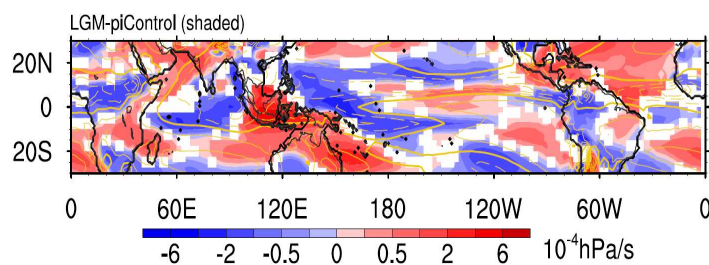
518



519

520 **Figure 3** (a) JJA mean precipitation (shading) difference and surface wind (vectors) difference  
 521 between LGME and piControl, and (b) the climatology of JJA mean precipitation (shading) and  
 522 surface wind (vectors) derived from piControl. The red lines enclose the monsoon domains. The  
 523 thick black lines in (a) denote the coastal lines in LGME, and the thin black lines denote the  
 524 coastal lines in piControl. Only those areas where signal-to-noise ratio exceeds one are plotted in  
 525 (a).

526

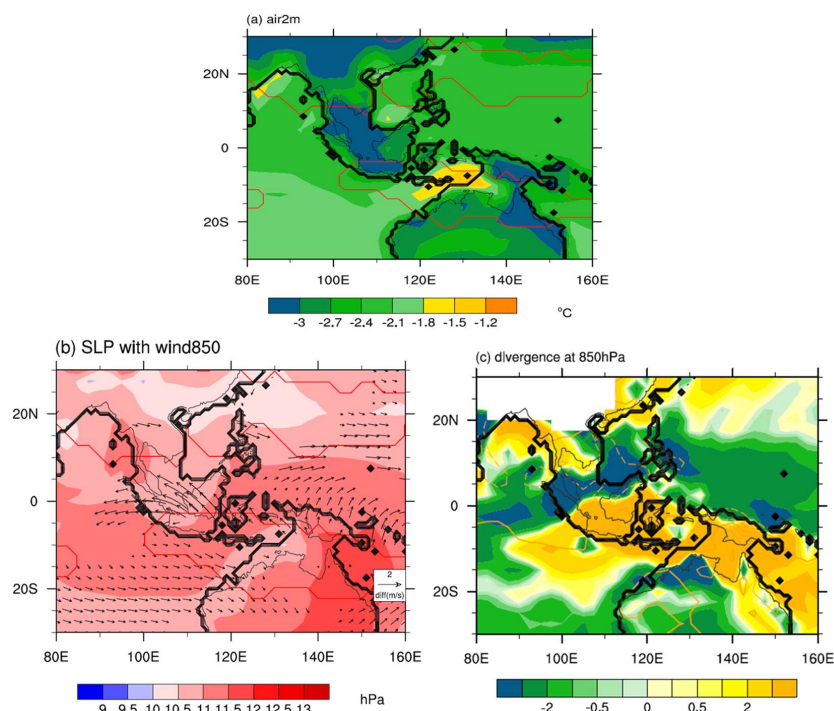


527

528 **Figure 4** The difference of JJA mean vertical velocity at 500 hPa between LGME and piControl  
 529 (in shading) and the corresponding climatology derived from piControl (yellow contours). The  
 530 thick black lines denote the coastal lines in LGME, and the thin black lines denote the coastal  
 531 lines in piControl. Only those areas where signal-to-noise ratio exceeds one are plotted in the  
 532 difference pattern.



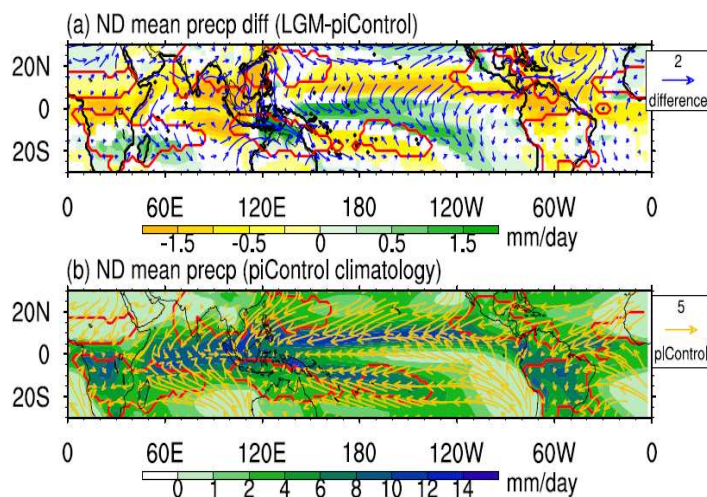
533



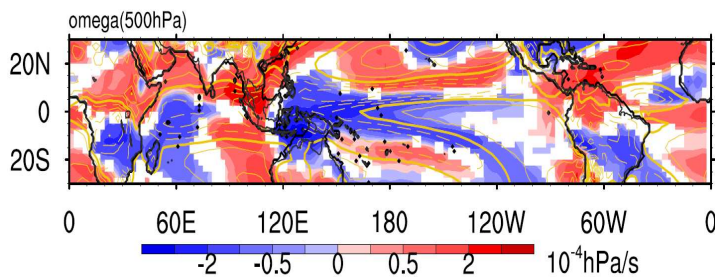
534

535 **Figure 5** JJA mean (a) surface air temperature, (b) sea level pressure (shading) with 850 hPa  
536 wind (vector), and (c) 850 hPa divergence differences between LGME and piControl. The red  
537 lines in (a) and (b) enclose the monsoon domains. The orange lines in (c) represent the  
538 climatology derived from piControl. The thick black lines denote the coastal lines in LGME, and  
539 the thin black lines denote the coastal lines in piControl. Only those areas where signal-to-noise  
540 ratio exceeds one are plotted.

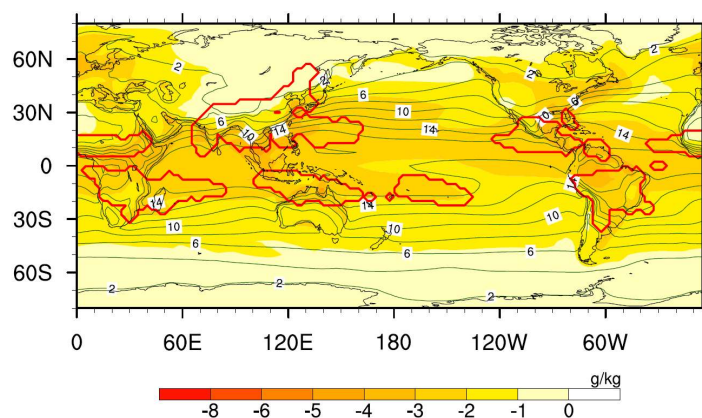
541



542  
543 **Figure 6** (a) ND mean precipitation (shading) difference and surface wind (vectors) difference  
544 between LGME and piControl, and (b) the climatology of ND mean precipitation (shading) and  
545 surface wind (vectors) derived from piControl. The red lines enclose the monsoon domains. The  
546 thick black lines in (a) denote the coastal lines in LGME, and the thin black lines denote the  
547 coastal lines in piControl. Only those areas where signal-to-noise ratio exceeds one are plotted in  
548 (a).  
549

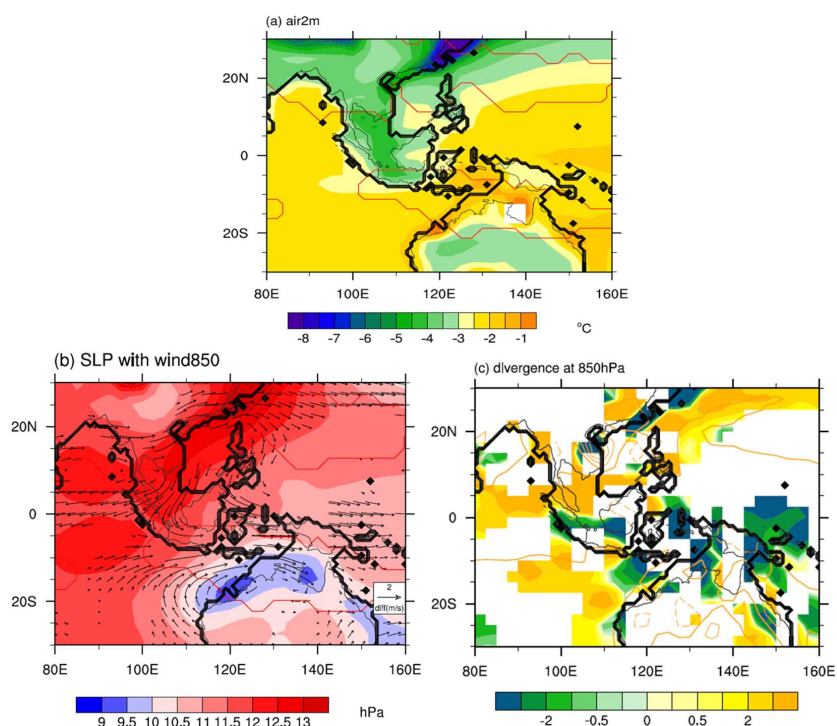


550  
551 **Figure 7** The difference of the ND mean vertical velocity at 500 hPa between LGME and  
552 piControl (in shading) and the corresponding climatology derived from piControl (yellow  
553 contours). The thick black lines denote the coastal lines in LGME, and the thin black lines denote  
554 the coastal lines in piControl. Only those areas where signal-to-noise ratio exceeds one are  
555 plotted in the difference pattern.  
556



557  
558 **Figure 8** Difference of ND mean surface specific humidity between LGME and piControl  
559 (shaded). The green contours denote the climatology derived from piControl. The red lines  
560 enclose the monsoon domains. Only those areas where signal-to-noise ratio exceeds one are  
561 plotted.  
562





563

564 **Figure 9** ND mean (a) surface air temperature, (b) sea level pressure (shading) with 850 hPa

565 wind (vector), and (c) 850 hPa divergence difference between LGME and piControl (shading).

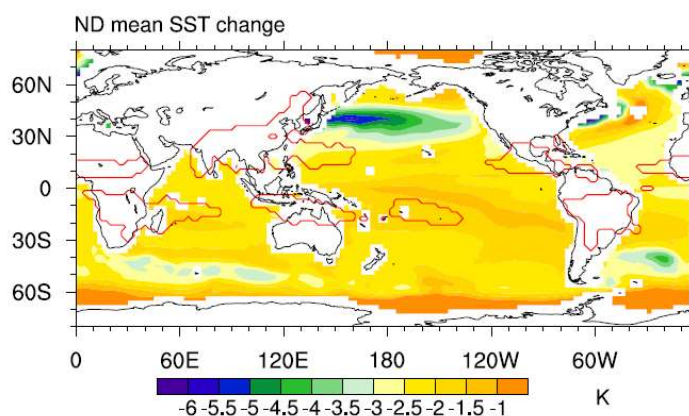
566 The red lines in (a) and (b) enclose the monsoon domains. The orange lines in (c) represents the

567 climatology derived from piControl. The thick black lines denote the coastal lines in LGME, and

568 the thin black lines denote the coastal lines in piControl. Only those areas where signal-to-noise

569 ratio exceeds one are plotted.

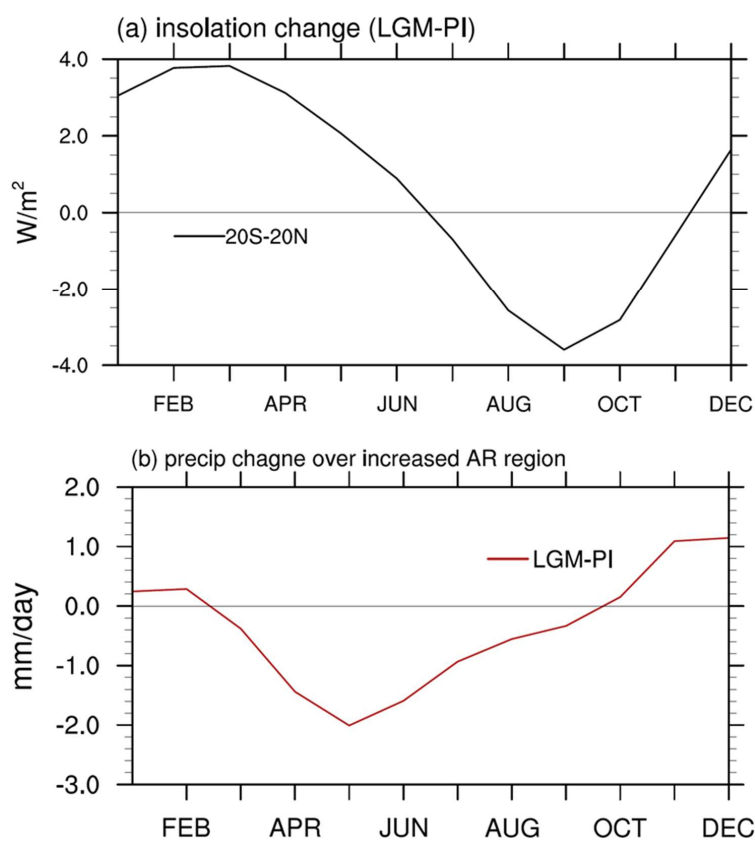
570



571

572 **Figure 10** ND mean SST difference between LGME and piControl. The red lines enclose the  
573 monsoon domains. Only those areas where signal-to-noise ratio exceeds one are plotted.

574



575

576

**Figure 11** Seasonal distribution of (a) insolation change between 20°S and 20°N, and (b)

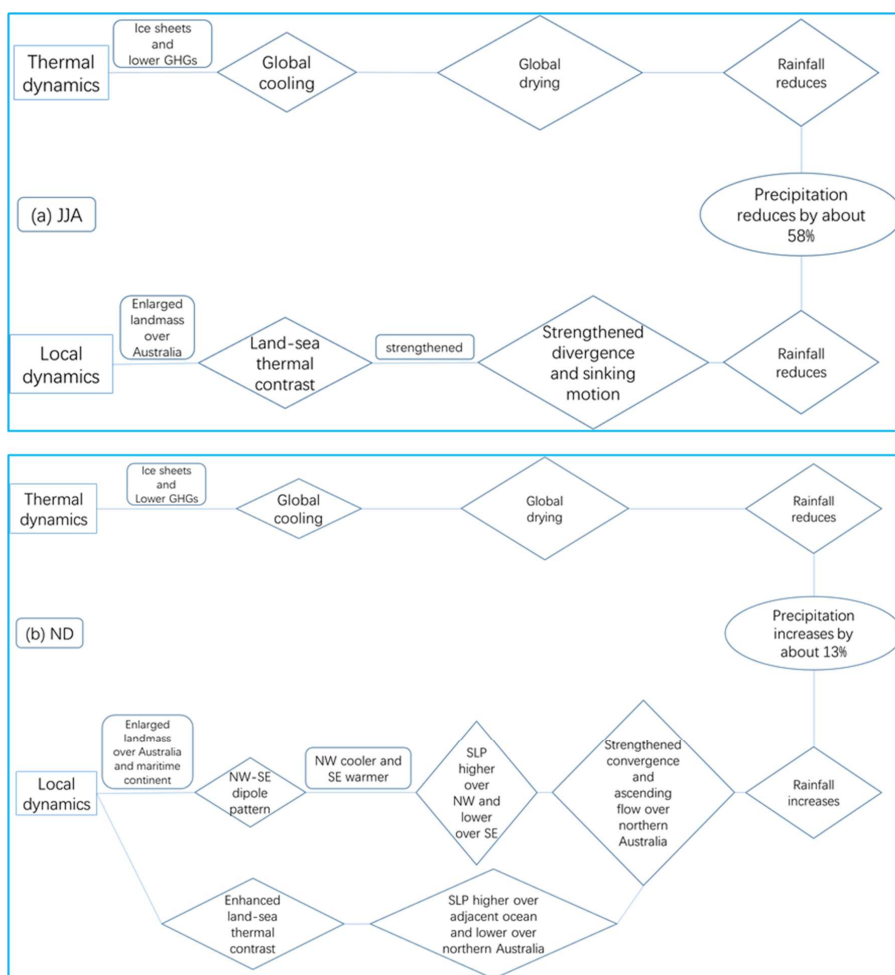
577

precipitation change over the central Australian monsoon region. The changes are calculated by

578

the LGM value minus the PI value.

579



580

581 **Figure 12** Mechanisms of Australian monsoon precipitation change (a) in JJA, and (b) in ND  
 582 during the LGM, in thermal dynamics and dynamics perspectives.

583

584

585



586 **Table 1** CMIP5/PMIP3 models and experiments used in this study.

Model	Institution	piControl Time span (years)	LGME Time span (years)	Spatial resolution for atmospheric module Lat × Lon Grids
CCSM4	National Centre for Atmospheric Research (NCAR)	501	101	288 × 192
CNRM-CM5	Centre National de Recherches Meteorologiques/Centre Europeen de Recherche et Formation Avancees en Calcul Scientifique (CNRM-CERFACS)	850	200	256 × 128
GISS-E2-R	NASA Goddard Institute for Space Studies (NASA GISS)	1200	100	144 × 90
IPSL-CM5A-LR	Institute Pierre-Simon Laplace (IPSL)	1000	200	96 × 95
MIROC-ESM	Atmosphere and Ocean Research Institute, University of Tokyo, National Institute for Environmental studies, and Japan Agency for Marine-Earth Science and Technology	531	100	128 × 64
MPI-ESM-P	Max Planck Institute for Meteorology	1156	100	196 × 98
MRI-CGCM3	Meteorological Research Institute (MRI)	500	100	320 × 160

587  
588  
589

**Table 2** Main changed boundary conditions used for the piControl and LGME experiments.

	piControl	LGME
<b>Orbital parameters</b>	Eccentricity = 0.016724 Obliquity = 23.446° Angular precession = 102.04°	Eccentricity = 0.018994 Obliquity = 22.949° Angular precession = 114.42°
<b>Trace gases</b>	CO <sub>2</sub> = 280 ppm CH <sub>4</sub> = 650 ppb N <sub>2</sub> O = 270 ppb	CO <sub>2</sub> = 185 ppm CH <sub>4</sub> = 350 ppb N <sub>2</sub> O = 200 ppb
<b>Ice sheets</b>	Modern	Provided by ICE-6G v2 (Peltier, 2009)
<b>Land surface elevation and coastlines</b>	Modern	Provided by PMIP3

590